Journal of Alloys and Compounds 386 (2005) 165–173

Journal of ALLOYS AND COMPOUNDS

www.elsevier.com/locate/jallcom

Detailed study of the crystallization behaviour of the metallic glass $Fe_{75}Si_9B_{16}$

K. Chrissafis, M.I. Maragakis, K.G. Efthimiadis, E.K. Polychroniadis*

Solid State Section, Physics Department, Aristotle University of Thessaloniki, GR-54124, Thessaloniki, Greece

Received 3 May 2004; received in revised form 24 May 2004; accepted 24 May 2004

Abstract

The crystallization behaviour of the metallic glass $Fe_{75}Si_9B_{16}$ was studied by means of transmission electron microscopy (TEM), differential scanning calorimetry (DSC) and magnetic measurements. A detailed interpretation of the results led to some interesting conclusions. The material is crystallised in three distinguished steps. During the first step, iron crystallises in two different forms, i.e. pure iron spherulites and Fe(Si) dendrites. High resolution TEM reveals some short-ranged order iron cluster which explains the two morphologies. The primary crystallization follows a homogeneous nucleation and diffusion-controlled three-dimensional growth. The other two steps (i.e. the eutectic crystallization of bcc Fe(Si) and bct Fe_3B plus the separation of Fe_3B into bcc Fe(Si) and bct Fe_2B and the independent crystallization of the bct Fe_2B from the amorphous matrix), as one peak in the DSC measurements, follow a homogenous nucleation and interface reaction controlled three-dimensional growth. Finally, a satisfactory coincidence of the DSC and magnetic curves was achieved, something which has to be emphasised, as it is being described for the first time.

Keywords: Amorphous materials; Scanning and transmission electron microscopy; Thermal analysis; Magnetic measurements

1. Introduction

Metallic glasses have attracted considerable attention due to their technologically interesting properties [1,2]. The most intensively studied glasses are the binary ones, especially $Fe_{1-x}B_x$ [3]. It has been found that the addition of Si to the Fe–B system enhances the thermal stability of the alloy [4]. More specifically the most favourable Fe–Si–B glasses concerning their thermal stability have 5–10 at.% Si and 75–78 at.% Fe and indeed, glasses with the greatest technological significance fall in this region [5]. Despite the great number of publications, the scientific community continues to study these materials proposing even recently specific applications [6]. But before any study for an application, detailed knowledge of their crystallization and kinetic behaviour is completely necessary, due to the amorphous (i.e. unstable) nature of the materials.

For Fe–Si–B amorphous alloys, the phases initially formed during heating, were dependent upon alloy composition and, in addition, great differences in crystallization morphology were found [7,8]. Nevertheless comprehensive studies both of the microstructures and the kinetics of the crystallization of $Fe_{75}Si_9B_{16}$ metallic glasses have not been yet undertaken. A detailed study of the crystallization behaviour of $Fe_{75}Si_9B_{16}$ is thus greatly needed for a better understanding of the material.

Contributing to this study, several members of the Fe–Si–B glass system with or without additives have been examined by different techniques. Thus, the thermal stability, the effective activation energy E_1 and the Avrami exponent n_1 of the different crystallization steps were determined, using differential scanning calorimetry (DSC) [9,10]. A study of high temperature magnetization and X-ray diffraction was performed [4] and finally several phases in the primary products of the first crystallization step as well as metastable and stable eutectic crystallization during the whole crystallization procedure were determined, using transmission electron microscopy (TEM) [11]. All the above-mentioned studies aimed at a better understanding of the influences of the alloy composition, annealing temperature and time of the crystallization procedure and the crystallization products. But this very important subject is not yet completed.

* Corresponding author. Tel.: +30-231-0998163; fax: +30-231-0998241.
E-mail address: polychr@auth.gr (E.K. Polychroniadis).

0925-8388/$ – see front matter © 2004 Elsevier B.V. All rights reserved.
doi:10.1016/j.jallcom.2004.05.062

In the present paper, the transformation from the amorphous to the crystalline state during heating of $Fe_{75}Si_9B_{16}$ is thoroughly investigated with TEM, DSC and magnetic measurements to elucidate the crystallization and kinetic behaviour of this metallic glass. This combination of the three independent methods of investigation allows us to go deeper into the study and explain better the experimental results. The detailed TEM study by in-situ heating under continuous observation gives the advantage of the immediate detection of any new crystallization feature which possibly might disappear or be obscured later by another crystallization process. Also, besides the study of the crystallization behaviour, an attempt is also undertaken to correlate the macroscopic properties of the material with the microscopic structural properties, always as a function of temperature. This led to a morphological coincidence of the thermal and magnetic curves detecting the same course of events, i.e. the crystallization process, but following the changes of completely different physical properties of the material.

2. Experimental procedure

Amorphous ribbons with composition $Fe_{75}Si_9B_{16}$ were prepared by the melt spinning method, while the ingots (as starting material) were prepared by arc-melting $3N^+$ pure materials in the appropriate percentages. The composition and homogeneity of the ribbons were verified by energy dispersive spectroscopic (EDS) analysis as regards Fe and Si, whereas the atomic concentration of B was taken as equal to the value calculated during the preparation of the ingots.

The electron microscopic study was carried out in a JEOL 100CX TEM, using a high voltage of 100 kV. The observations followed the in situ heating up to 650 °C and so, the whole study was performed under high vacuum. Starting

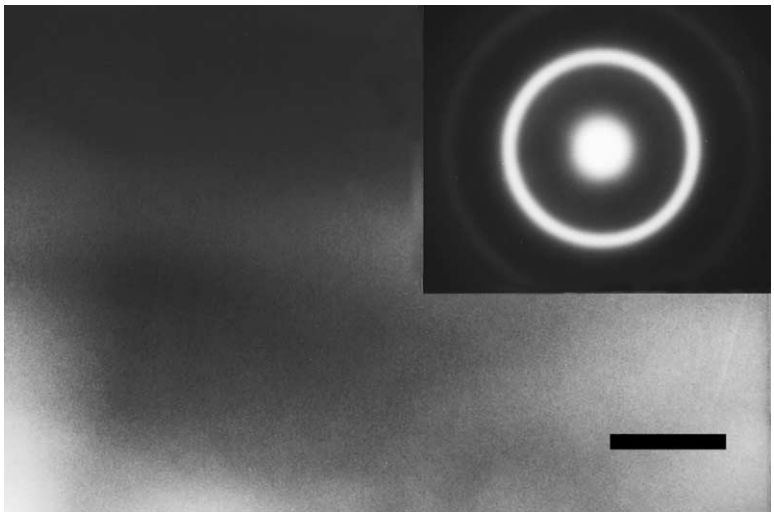

Fig. 1. The absence of any contrast in the conventional electron micrograph at room temperature, as well as the characteristic halo in the corresponding diffraction pattern, confirms the amorphous nature of the material (bar = 0.5 μm).

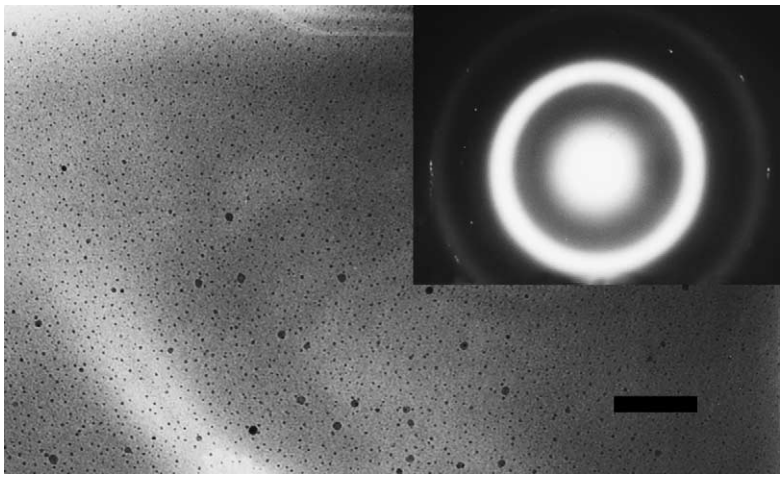

Fig. 2. Small iron spherulites formed during the initial stage of crystallization (bar = 0.2 μm).

from room temperature, every 25 °C the specimen was left to thermally stabilise for half an hour and then the observation took place and the necessary micrographs were obtained. The high resolution electron microscopic observation was carried out in a JEOL 2010 TEM, using an accelerating voltage of 200 kV. Several specimens were prepared and the TEM observation with in situ heating was repeated several times in order to exclude the presence of artifacts which are not rare in this kind of experiments.

The saturation magnetization (at $B = 0.5$ T) was measured with a vibrating sample magnetometer; the samples were ribbon fractions with a total mass of approximately 30 mg. The measurements were made either during the heating of the samples from room temperature up to 800 °C at a rate of 3 °C/min or during a 24-h heating at constant temperature, where the rate until the particular temperature was reached was 10 °C/min. All the measurements were performed two or three times, to minimise errors, mainly introduced by possible non-homogeneity of the ribbons.

The thermal behaviour of the materials was investigated, using a Setaram DSC 131 differential scanning calorimeter. Temperature and energy calibrations of the instrument were performed, using the well-known melting temperatures and melting enthalpies of high purity zinc and indium, supplied with the instrument. The samples, weighing about 10 mg, were crimped in stainless steel crucibles and an empty stainless steel crucible was used as reference. This study was performed either by non-isothermal DSC runs by heating the specimens from room temperature up to 700 °C with heating rates varying from 2.5–20 K min^{-1} or by isothermal measurements at constant temperatures, varying from 491 to 521 °C.

3. Results and interpretation

3.1. TEM observations

The microstructural study of the crystallization procedure was performed during in situ heating in the TEM. Bright field images of the as-grown material show a homogeneous featureless contrast and the corresponding selected area diffraction pattern confirms the amorphous nature of the material (Fig. 1). The heating of the sample reveals three distinct stages of crystallization.

During the initial stage of crystallization, small iron spherulites are formed, which are evenly distributed all over the amorphous matrix (Fig. 2). Nearly at the same time, at an early stage, a portion of the amorphous iron forms Fe(Si) crystallites in its most common form, the dendritic one (Fig. 3). The appearance of two distinct morphologies of iron crystallites, as well as the difference in their growth mode can be due to the fact that the small iron shperulites that are initially formed, contain much less Si than the dendrites that appear afterwards. The first ones are probably formed because of the pre-existing nano-nuclei of iron in the bulk. Around them, the material is richer in Si concentration and this, therefore, leads to the crystallization of the second dendritic form of Fe(Si).

The nature of the material before the heat treatment, together with the strong tendency of the as-grown alloy to form a crystalline structure is also the most probable explanation for the observed different behaviour of the iron to be

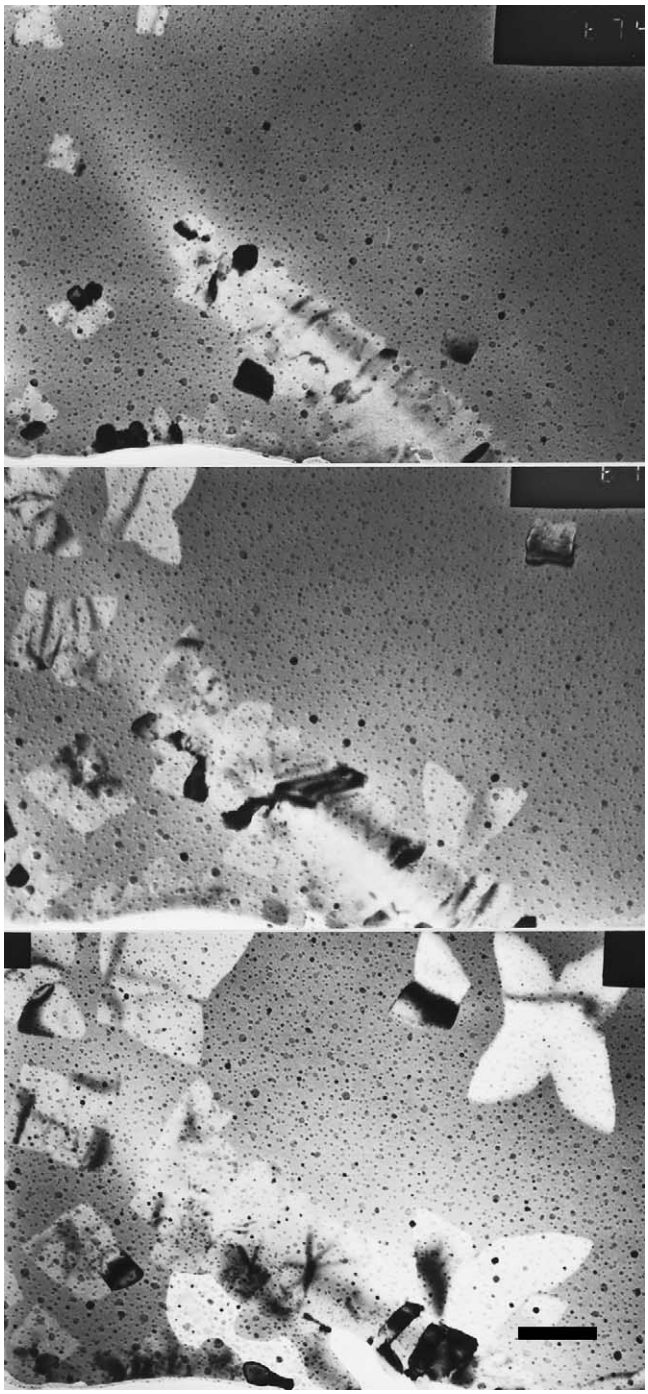

Fig. 3. A sequence of TEM micrographs showing the crystallization of Fe(Si) in their dendritic form. While the nucleation rate is minimised, the growth rate is high (bar = 0.2 μm).

crystallised. The reason is that the spherulites appear simultaneously in all the volume of the material far away from any kind of surface crystallization, contrary to the dendrites which started to develop at the edge of the thinned specimen (i.e. the thinner part of the specimen). This means that although the time interval between the appearances in TEM of the two different iron morphologies is practically zero, the dendrites appear at a higher temperature. The simultaneous appearance is due to the minimum thickness of this region, where the influence of the surface is predominant as the portion of surface atoms is maximum. This is in agreement with the already-mentioned higher thermal stability of the amorphous Fe(Si) in comparison with the pure metal.

In order to verify the idea of the pre-existing iron nuclei in the as grown material, a high resolution observation was realised (Fig. 4). Indeed in this high resolution electron micrograph several one-dimensional lattice images were observed having a spacing of about 0.20 nm in the form of small groups of fringes. The spacing of the 0.20 nm lattice fringes corresponds to the {1 1 0} planes of the bcc a-Fe as well as to the inverse distance between the central spot and the first halo ring in the diffraction pattern. From these observed lattice fringes, it is presumed that the observed small crystalline domains are iron nuclei that exist in the initial as quenched amorphous alloy. It is known that for observation of lattice images by TEM only rows of atoms which are very closely parallel to the incident beam give rise to fringes in the high resolution image. For this reason, it is possible that additional ordered regions exist in the other areas where fringes are not observed. It is possible that these ordered regions can act as embryos for subsequent crystallization of the alloy during heat treatment. On the other hand, it is sure that these short-range ordered clusters exist prior to the heat treatment, are surrounded by the amorphous matrix and form a complicated non-equilibrium solid structure. So, it is also possible for this "structure" to crystallise at temperatures lower than that of the equilibrium crystallization of the matrix. Furthermore, it is useful to notice that the observed fringes are not preparation artifacts and are not created during the ion milling due to the low energy Ar ions bombardment because a special accessory (with liquid nitrogen) was used to keep the specimen temperature below 0 °C.

As the heating continues, at the second stage of the crystallization, which starts at slightly higher temperature, nuclei of the metastable bct Fe_3B crystallites appear. These nuclei have a eutectic composition of bcc Fe(Si) and bct Fe_3B (Fig. 5) and are intensely found between the dendrite branches, where there is an abundance of B. The crystallization is completed in the third stage which starts right after the second one and in which the metastable bct Fe_3B phase separates into bcc Fe(Si) and bct Fe_2B (Fig. 6). These are of course the finally traceable crystals after a high temperature heating.

3.2. Magnetic measurements

The study of the magnetization as a function of temperature as well as the isothermal variation of the magnetization at selected temperatures, are convenient and helpful ways to follow the crystallization of the amorphous alloys during heating.

Fig. 7 shows the variation of the specific magnetization as a function of temperature, when the rate of rise of the latter is 3 °C/min. Under these conditions, the critical temperatures (points of curvature resulted from the first derivative of specific magnetization) are: $T_c = 440$ °C (Curie temperature), $T_{x1} = 538$ °C (temperature of first crystallization) and $T_{x2} = 545$ °C (temperature of second crystallization).

Fig. 8 shows the isothermal variation of the specific magnetization at selected temperatures. These measurements suggest that the crystallization of amorphous $Fe_{75}Si_9B_{16}$ is manifested in three stages. During its 24-h heating at 400 and 425 °C only the first stage of crystallization takes place.

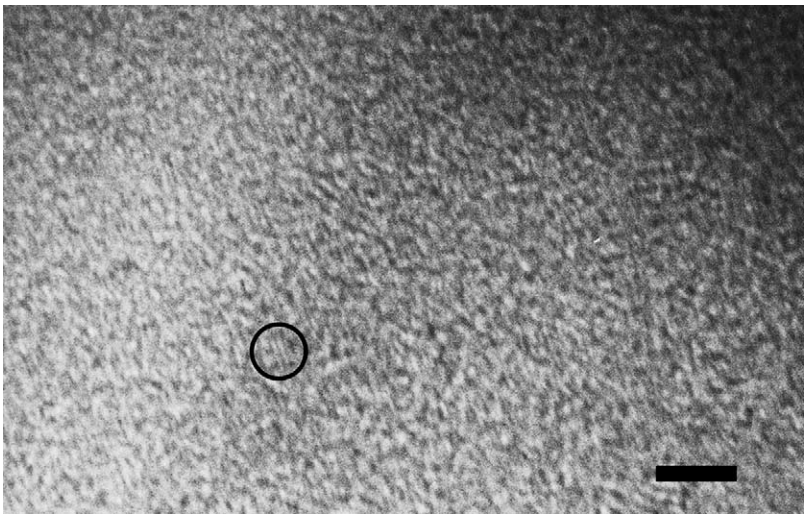

Fig. 4. High resolution bright field image of the as quenched amorphous alloy, where fringes are visible indicating iron nuclei (bar = 2 nm).

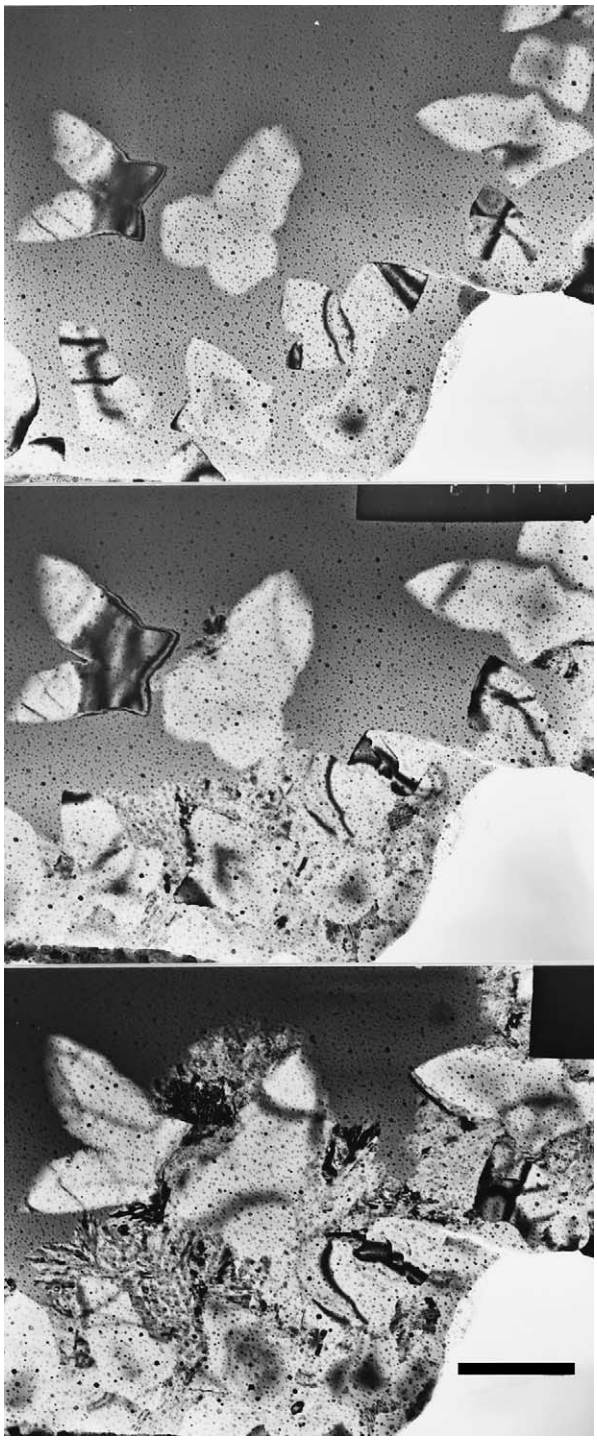

Fig. 5. A sequence of TEM micrographs showing the eutectic crystallization of bcc Fe(Si) and bct Fe_3B. In this crystallization stage, the growth rate of Fe(Si) dendrites is reduced, while the eutectic crystallization keeps a high growth rate. It is easily shown that this crystallization starts between the iron dendrite branches (bar = 0.5 μm).

After 8 h of heating at 450 °C starts the second stage. The third stage is evident after a 6-h heating of the material at 475 °C, where at 500 °C the whole crystallization procedure is over in 2 h.

3.3. Differential scanning calorimetry

3.3.1. Dynamic heat treatment

A series of DSC experiments was carried out with continuous heating rates in the range 2.5–20 K min^{-1}. The crystallization of the glassy sample has always appeared by at least two overlapping exothermic peaks (Fig. 9). In addition, the shape of the overall thermogram was strongly dependent on the heating rate.

It is clearly visible that the ratio of the heights of the two peaks which are always present in the thermogram increases continuously with the heating rate. At the heating rate β =2.5 K min^{-1} the second peak is much higher than the first one (curve 1 in Fig. 8), at the heating rate $\beta = 5$ K min^{-1} the two peaks are almost equal (curve 2), while in the two other curves (curves 3 and 4 in Fig. 8, at heating rates 10 and 20 K min^{-1}), the first peak is much greater than the second one. It is evident that the first peak-associated always with the primary crystallization becomes more prominent than the second one, with the increasing of the heating rate, something that has already been observed [12]. Unfortunately, due to the great overlapping of the peaks, which is also increasing by increasing the heating rate, it is not possible to separate the peaks unambiguously, using one of the known specified software. This hampered the possibility of an independent kinetic analysis for each peak. The situation becomes more complicated for heating rates above 6 K min^{-1}, where also a third peak possibly exists. This third peak finally disappears at the heating rate 20 K min^{-1}, giving rise to a heat flow plateau after the first peak. Independently of the peak morphology, the total enthalpy remains almost constant for all heating rates, having a mean value of 170 kJ/mol.

3.4. Isothermal heat treatment

The isothermal DSC experiments were carried out at temperatures T_a lying in the range 491–521 °C which is related to the onset temperature of the first dynamic crystallization DSC peak ($T_x = 541$ °C at $\beta = 10$ K min^{-1}). As shown in Fig. 10, two overlapping exothermic peaks were always observed.

In this case, the overlapping is limited and the two peaks can be distinguished from each other. For this reason, their mathematical separation is reliable and was realised, using peak separation software. Thus, the crystallization enthalpy was calculated not only for the overall transformation but even for each one of the two peaks. The results are given in Table 1, where as it can be seen, the total enthalpy is almost constant independently of the annealing temperature having a mean value of 159 kJ/mol. The other two enthalpies for the two separated peaks vary and the enthalpy calculated from the first peak increases as the annealing temperature increases contrary to the enthalpy calculated from the second peak which decreases as the annealing temperature increases. In Table 1, the ratios of the two enthalpies

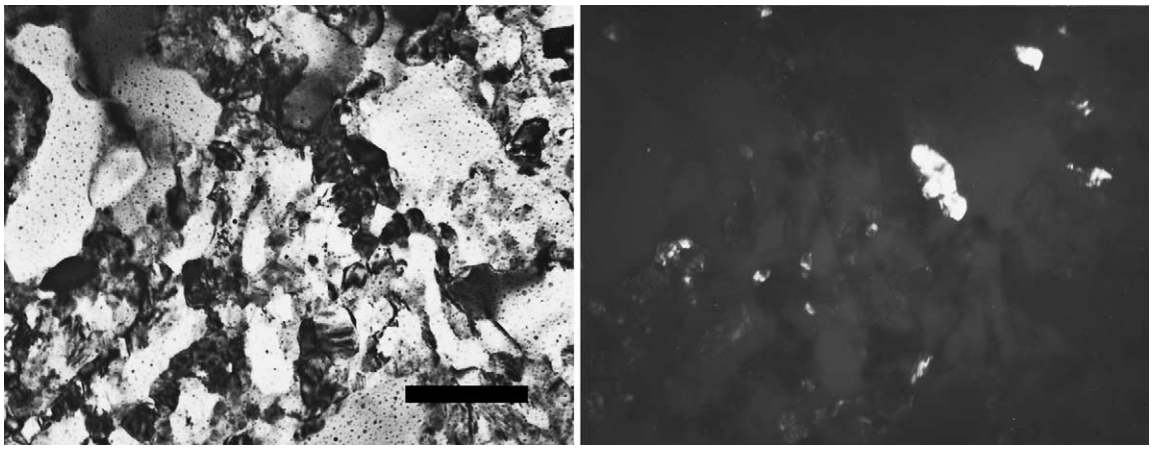

Fig. 6. Bright and dark field TEM images showing the third crystallization stage where the bct Fe_2B starts to grow (bar = 0.5 μm).

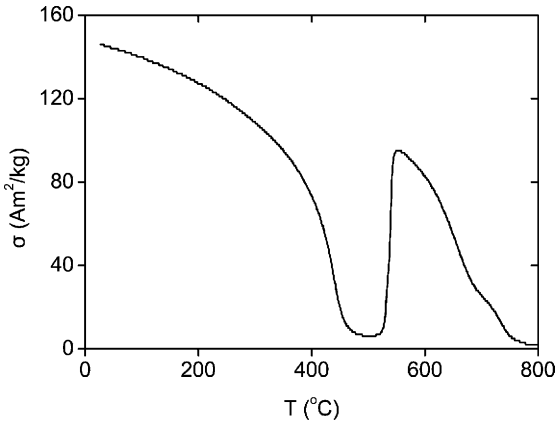

Fig. 7. Specific magnetization (at $B = 0.5$ T) during heating at the constant heating rate of 3 K min^{-1}.

calculated from the two separated peaks in each annealing temperature are also presented. As it is seen this ratio increases with temperature increase. A similar behaviour has also been observed for the non-isothermal treatments for the ratio of the peak highs in relation to the heating rates.

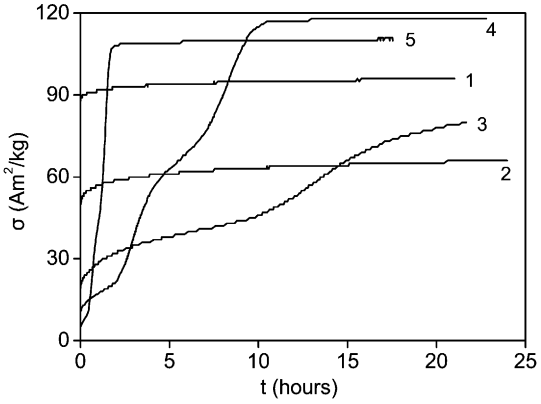

Fig. 8. Isothermal variation of the specific magnetization at different temperatures. (1): 400 °C, (2): 425 °C, (3): 450 °C, (4): 475 °C, (5): 500 °C.

Table 1
Isothermal enthalpies (H_1, H_2) calculated from the two separated peaks in each annealing temperature, the ratio of the two and the sum of them

T (°C)	H_1 (J/g)	H_2 (J/g)	H (J/g)	H_1/H_2
496	29.1	125.9	155.0	0.23
501	34.1	129.6	163.7	0.26
506	37.9	117.1	155.0	0.32
511	43.8	112.4	156.2	0.39
516	51.8	112.1	163.9	0.46
521	60.2	99.4	159.6	0.61

4. Kinetic analysis

For the study of crystallization kinetics the following assumption was undertaken: each crystallization peak can be described by a kinetic equation of the form:

$$\frac{d\alpha}{dt} = k(T)\, f(\alpha) \tag{1}$$

where

$$k(T) = A \exp\left[-\frac{E}{(R/T)}\right] \tag{2}$$

is the Arrhenius temperature-dependent rate constant, E is the apparent activation energy, A is the pre-exponential factor and $f(\alpha)$ characterises the type of transformation mechanism.

The activation energy of crystallization (E) was calculated from the non-isothermal measurements, using the Kissinger's method [13], which relates the dependence of T_p on heating rate β through the following equation:

$$\ln\left(\frac{\beta}{T_p^2}\right) = -\frac{E}{RT_p} + \ln\left(A\frac{R}{E}\right) \tag{3}$$

The value of E (kJ/mol) was obtained from the slope of $\ln(\beta/T_p^2)$ versus $1000/T_p$ plot given in Fig. 11 and the pre-exponential factor A (s^{-1}) from the intercept. The activation energy for the first peak is 445 ± 18 kJ/mol and for

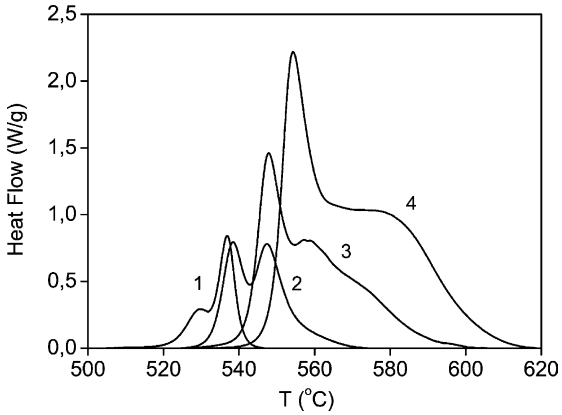

Fig. 9. DSC linear heating curves of $Fe_{75}Si_9B_{16}$ with continuous heating rates. (1): 2.5 K min^{-1}, (2): 5 K min^{-1}, (3): 10 K min^{-1}, (4): 20 K min^{-1}.

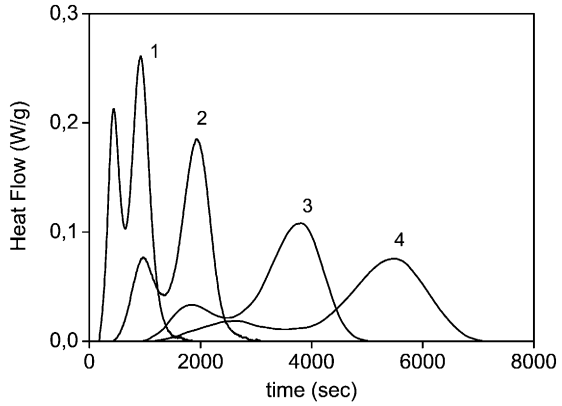

Fig. 10. Isothermal DSC crystallization curves at different temperatures. (1): 521 °C, (2): 511 °C, (3): 501 °C, (4): 496 °C.

the second peak is 363 ± 8 kJ/mol. It is seen that the activation energy of the first peak is greater than the one of the second peak, something which has been already observed at the Fe–Si–B metallic glasses [14,15].

The crystallization kinetics is usually interpreted in terms of the standard nucleation—growth model formulated by Johnson–Mehl–Avrami (JMA) [16]. This model describes

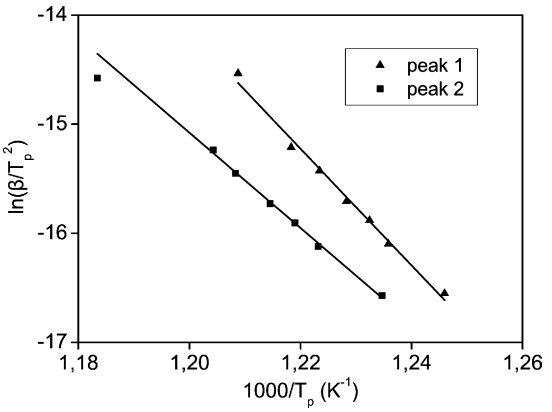

Fig. 11. The Kissinger plots of the heating rate shift in the DSC peak temperature.

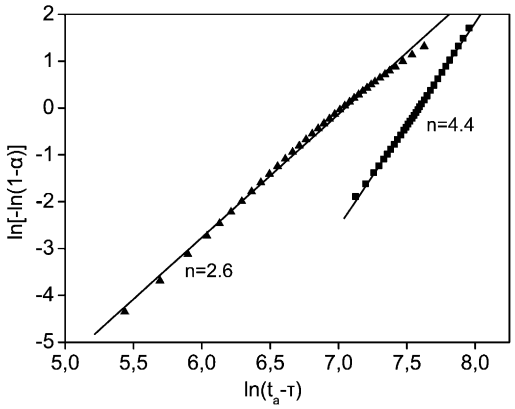

Fig. 12. The calculated JMA plots of the two (first (▲) and second (■), respectively) isothermal crystallization peaks for $T = 501\,^{\circ}C$. Time lag τ is equal to 955 and 1885 s, respectively.

the time dependence of the fractional extent of reaction α, usually written in the following form:

$$\alpha = 1 - \exp[-(kt)^n] \quad (4)$$

where the kinetic exponent n is a parameter which reflects the nucleation frequency and/or the growth morphology. In the isothermal case [17], the Eq. (4) becomes

$$\ln(-\ln(1-\alpha)) = n \ln[k(T)] + \ln t \quad (5)$$

If the assumed linearity is not observed, then some time lag, τ, can be found for each isotherm and subtracted from the real experimental time, t, to linearize Eq. (5) following the Thompson, Greer and Spaepen procedure [18]. This mathematical formalism is equivalent to the assumption of the existence of transient nucleation rate in the JMA kinetics.

Fig. 12 presents representatively the JMA plots for the two isothermal crystallization peaks for $T = 774$ K (501 °C), where the kinetic exponent was calculated to be $n = 2.6$ and $n = 4.4$, respectively. Table 2 includes the n values for both peaks for all the annealing temperatures. As it is seen, the n value for the first crystallization peak is always close to 2.5, which means that the primary crystallization follows a homogeneous nucleation and diffusion-controlled three-dimensional growth [19]. For the second crystallization peak, n is slightly above 4 which means that the completion of the crystallization follows a homogeneous nucleation and interface reaction controlled three-dimensional growth [19].

Table 2
Calculated linearization fitting parameters for the two isothermal peaks for a temperature range 496–516 °C

T (°C)	n_1	n_2
496	2.5	4.3
501	2.6	4.4
506	2.9	4.7
511	3.0	4.1
516	2.9	3.9

5. Discussion and conclusions

The advantage of the TEM study of crystallization, already described, by in situ slow rate heating is that it elongates the time period of the crystallization. Consequently, as the crystallization procedure itself is very slow, at constant temperature, TEM observations are able to distinguish the different crystallization steps. The use of other indirect methods, such as magnetic measurements or thermal analysis, although sensitive to the crystallization procedure, are difficult to point out the details of the crystallization, due to the fact that all the steps take place almost simultaneously and there is always overlapping of the corresponding curves. So, the combination of different independent methods of investigation, although they are sometimes difficult to be compatible, always gives a better understanding and a deeper view of the whole procedure of the crystallization.

The three crystallization stages as they were concluded by both the TEM study and the magnetic measurements could be the final statement concerning the crystallization sequence. These, focused by the new detailed study, are:

1. The crystallization of the bcc Fe in the two morphologies. The volume ratio of the small spherulites that appear first and remain almost unchanged during heating is too small to be detectable by the other methods of investigation. So, this stage is mainly represented by the clear and characteristic appearance of the iron dendrites.
2. The eutectic crystallization of bcc Fe(Si) and bct (Fe_3B) which starts at the deepest place between the iron branches, where it is estimated that the higher concentration of B exists.
3. The crystallization of the bct Fe_2B, after the decomposition of the metastable Fe_3B phase or directly from amorphous mass. This third stage of crystallization which follows immediately after the second one is not easily separated from the second one because it can also start independently in the amorphous matter and it does not necessarily pass through the other metastable iron borides (Fe_3B, $Fe_{3.5}B$, $Fe_{23}B_6$, etc.). So, the last two stages (second and third) appear almost always simultaneously and their corresponding curves at the measurements plots are almost overlapping.

All the above, concern the qualitative approach of the crystallization as it could be described after the TEM observations. But the magnetic measurements as well as the thermal analysis produce quantitative results which are expressed by the corresponding curves. From the moment that both methods of investigation describe the same physical phenomenon, these curves have to be in morphological coincidence. As it is known, the magnetization of an amorphous material is increased during crystallization. During this procedure, the specific magnetization is always the sum of the specific magnetization of the amorphous material and of the crystallization products. At temperatures where the crystallization is detected, the amorphous material is paramagnetic i.e. insignificant magnetization and so the measured one is due to the crystallization products (bcc Fe, bct Fe_3B and bct Fe_2B) which are ferromagnetic. So, the specific magnetization variation expresses mainly the crystallization evolution.

During the heating at constant rates, the specific magnetization is temperature dependent (a magnetic order-disorder phenomenon) but also is time dependent (due to the crystallization). So, the experimentally resulted temperature dependent specific magnetization $d\sigma/dT$ can be described by the following expression:

$$\frac{d\sigma}{dT} = \frac{\partial\sigma}{\partial T} + \frac{\partial\sigma/\partial t}{\partial T/\partial t}$$

The partial derivative, $\partial\sigma/\partial T$ expresses the variation due to magnetic order-disorder, while $\partial\sigma/\partial t$ expresses the variation due to the crystallization.

As it is mentioned, the measured variation of the specific magnetization is due to the crystallization products. Moreover, the Curie temperatures of all these products (bcc Fe: 770 °C, bct Fe_3B: 550 °C and bct Fe_2B: 740 °C) are higher than the temperature used in the experiments. The specific magnetization is highly varied near the Curie temperature and the variation is small at lower temperatures. So, the partial derivative $\partial\sigma/\partial t$ in a first approximation can be estimated to be much lower than the partial derivative $\partial\sigma/\partial t$ which representing the nucleation and growth procedure. Consequently, the experimentally resulting $d\sigma/dT$ which is mainly time-dependent can be compared with the heat flow.

For this reason, instead of having the variation of saturation magnetization (σ), as a function of temperature (Fig. 7), its first derivative with respect to temperature, $d\sigma/dT$ was calculated and is presented versus temperature in Fig. 13 (curve 1). This curve, using similar heating rates is compared in the same figure with the variation of the heat flow versus temperature as derived by the DSC measurements during the linear heating treatment (curve 1 in Fig. 9 and curve 2 in

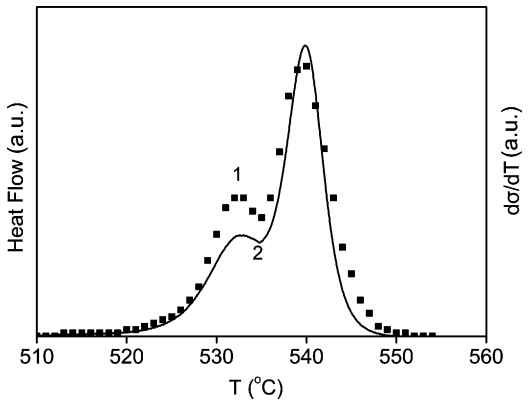

Fig. 13. Comparison between the temperature dependent specific magnetization $d\sigma/dT$ with the heat flow during the heating at constant rates. (1): $d\sigma/dT$ for heating rate $3\,K\,min^{-1}$, (2): heat flow for heating rate $2.5\,K\,min^{-1}$.

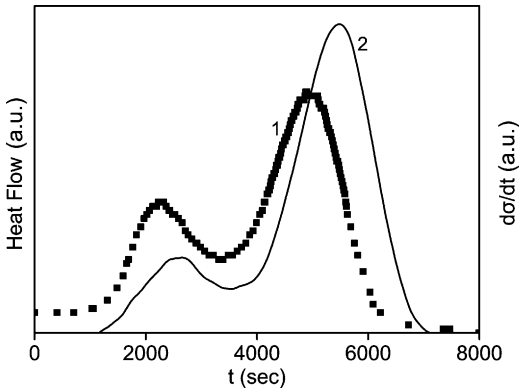

Fig. 14. Comparison between the time dependent specific magnetization $d\sigma/dt$ with the heat flow during the isothermal heat treatment. (1): $d\sigma/dt$ at constant temperature $T_a = 500\,^{\circ}C$, (2): heat flow at constant temperature $T_a = 496\,^{\circ}C$.

Fig. 13). Although, there is a small difference in the heating rate (3 °C/min for magnetic measurements and 2.5 °C/min for DSC), the morphological coincidence is obvious.

During the isothermal heat treatment, the time dependent specific magnetization $d\sigma/dt$ ($Am^2/kg\,s$) can be directly compared with the heat flow (J/kg s). So, instead of having the variation of the saturation magnetization (σ), as a function of time at constant temperature (curve 5 in Fig. 8), its first derivative with respect to time $d\sigma/dt$ was calculated and is presented versus time in Fig. 14 (curve 1). This curve is compared in the same figure with the variation of the heat flow versus time as derived by the isothermal heat treatment of the DSC measurements (curve 4 in Fig. 10 and curve 2 in Fig. 14). Also, in these two curves, although there is a small difference in the constant temperature ($T = 500\,^{\circ}C$ for magnetic measurements and $T = 496\,^{\circ}C$ for DSC), the similarity is again obvious.

Also, these two morphological coincidences of the curves, coming from completely independent methods of investigation, although they were in principle expected, they were experimentally realised for the first time. Despite the satisfactory match of the DSC and magnetic measurements, the last two figures present the complete three-stepped crystallization procedure with two peaks. This can be explained either by the relatively high heating rates or by annealing at relatively high temperatures. So, the two stages (second and third) can not be separated, as it has already been explained.

Conclusively, besides the three crystallization steps, electron microscopy explains the two different morphologies under which the first iron crystallites appear. DSC interpretation reveals that the primary crystallization follows a homogenous nucleation and diffusion-controlled three-dimensional growth, as well as the other two steps follow a homogeneous nucleation and interface reaction controlled three-dimensional growth. Moreover, the total enthalpy of the whole crystallization process was found to be 170 kJ/mol.

Finally, we can emphasise the supplementary effect of the three methods used for the detailed study of the crystallization as well as the final coincidence of their results.

References

[1] J. Arcas, M. Vasquez, A. Hernando, C. Gomez-Polo, Sens. Actuators A59 (1997) 101.
[2] H. Chiriac, E. Hristoforou, M. Neagu, I. Darie, V. Nagacevschi, Mater. Sci. Eng. A 226 (1997) 1093.
[3] Y. Khan, E. Kneller, M. Sostarich, Z. Metallkde. 72 (1981) 553.
[4] R. Singhal, A.K. Majumdar, J. Magn. Magn. Mater. 115 (1992) 245.
[5] I. Matko, E. Illekova, P. Svec, P. Duhaj, Mater. Sci. Eng. A 225 (1997) 145.
[6] H. Chiriac, C.S. Marinescu, Sens. Actuators 81 (2000) 174.
[7] M.A. Gibson, G.W. Delamore, J. Mater. Sci. 27 (1992) 3533.
[8] M.-S. Leu, J.S.C. Jang, C.-C. Lin, W.-K. Wang, Mater. Chem. Phys. 45 (1996) 275.
[9] V.R.V. Ramanan, G.E. Fish, J. Appl. Phys. 53 (1982) 2273.
[10] S. Surinach, M.D. Baro, N. Clavaguera, Z. Phys. Chem. Neue Folge 157 (1988) 395.
[11] M.A. Gibson, G.W. Delamore, Acta Metall. Mater. 38 (1990) 2621.
[12] E. Illekova, Thermochim. Acta 280–281 (1996) 289.
[13] H.E. Kissinger, J. Res. Nat. Bur. Stand. 57 (1956) 217.
[14] C.F. Chang, J. Marti, J. Mater. Sci. 18 (1983) 2297.
[15] P. Tomic, M. Davidovic, J. Non-Cryst. Solids 204 (1996) 32.
[16] E. Illekova, I. Matko, P. Duhaj, F.-A. Kuhnast, J. Mater. Sci. 32 (1997) 4645.
[17] E. Illekova, Thermochim. Acta 282–283 (1996) 91.
[18] C.V. Thompson, A.L. Greer, F. Spaepen, Acta Metall. 31 (1983) 1883.
[19] J.W. Christian, The Theory of Transformation in Metals and Alloys, second ed., Pergamon Press, NY, 1975 (Chapter 12).